THE JOURNAL OF PHYSICAL CHEMISTRY Letters

Letter

Cite This: J. Phys. Chem. Lett. 2018, 9, 2127−2132

pubs.acs.org/JPCL

Non-Plasmonic SERS with Silicon: Is It Really Safe? New Insights into the Optothermal Properties of Core/Shell Microbeads

Nicolò Bontempi,[†,∥] Irene Vassalini,[†,‡] Stefano Danesi,[†,‡] Matteo Ferroni,[§,∥] Maurizio Donarelli,[§] Paolo Colombi,[⊥] and Ivano Alessandri*[,†,§,∥]

[†]INSTM-UdR Brescia, via Branze 38, 25123 Brescia, Italy

[‡]Department of Mechanical and Industrial Engineering, University of Brescia, via Branze 38, 25123 Brescia, Italy

[§]Department of Information Engineering, University of Brescia, via Branze 38, 25123 Brescia, Italy

[∥]INO−CNR, via Branze 38, 25123 Brescia, Italy

[⊥]CSMT, via Branze 45, 25123 Brescia, Italy

Supporting Information

ABSTRACT: Silicon is one of the most interesting candidates for plasmon-free surface-enhaced Raman scattering (SERS), because of its high-refractive index and thermal stability. However, here we demonstrate that the alleged thermal stability of silicon nanoshells irradiated by conventional Raman laser cannot be taken for granted. We investigated the opto-thermal behavior of SiO_2/Si core/shell microbeads (Si-rex) irradiated with three common Raman laser sources (λ = 532, 633, 785 nm) under real working conditions. We obtained an experimental proof of the critical role played by bead size and aggregation in heat and light management, demonstrating that, in the case of strong opto-thermal coupling, the temperature can exceed that of the melting points of both core and shell components. In addition, we also show that weakly coupled beads can be utilized as stable substrates for plasmon-free SERS experiments.

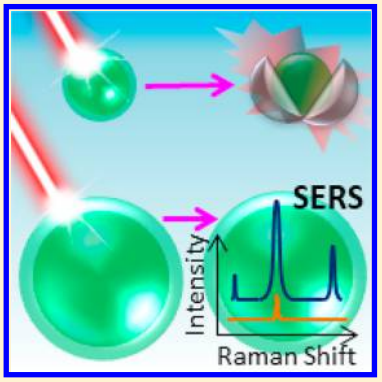

All-dielectric and semiconductor-based optical antennas are intensively investigated as promising substrates for surface enhanced Raman scattering (SERS).[1] This emerging interest stems from several factors. One is the possibility to exploit a rich variety of parameters to tune the Raman response. For example, the chemical enhancement can be widely modulated by controlling charge transfer and adsorption-induced changes of the molecular polarizability of a given analyte. In parallel, the electromagnetic enhancement can take advantage of Mie-type resonances, light trapping, and related optical effects to increase sensitivity and selectivity of the Raman response. Further major benefits of nonplasmonic SERS are low-invasiveness (plasmonic heating and plasmon-driven catalysis are avoided)[2−6] and high reproducibility, which make dielectrics more advantageous than metals for many types of Raman analysis, including the real-time monitoring of chemical reactions. These hallmarks are ultimately related to the lossless nature of dielectrics, which avoids the generation of strong local heating under light irradiation. Among the different types of dielectrics and semiconductors that have been proposed so far, SiO_2/TiO_2 core/shell beads (T-rex)[7] demonstrated unique performances in sensing environmental pollutants and biomarkers.[8−11] In particular, micron-sized beads can be individually visualized by optical microscopy and exploited as Mie resonators able to act as all-in-one colloidal platforms combining SERS, mass spectrometry and optical sensing.[12] As the SERS efficiency of these resonators is closely related to the refractive index contrast between core and shell, the replacement of the TiO_2 with a higher index material could further improve the performance of these systems.[13] In this regard, Si represents a natural choice in terms of high refractive index ($n \sim 4$ at the most common Raman exciting wavelengths) and compatibility with sensing devices.[14−16] Maier and co-workers demonstrated that dimers of spheres and nanodisks, either made of GaP or Si, are able to produce a good near-field enhancement, yet with minimal heating losses if compared with the analogous gold counterparts.[17,18] Moreover, Si nanoparticles can exhibit both electric and magnetic Mie resonances by direct excitation in the visible range, which could open interesting perspectives for developing silicon-based SERS-active metamaterials.[19]

Here we investigate for the first time the optothermal behavior of SiO_2/Si core/shell microbeads (Si-rex) irradiated with three common Raman laser sources (λ = 532, 633, 785 nm) under real working conditions. We obtained an experimental proof of the critical role played by bead size and aggregation in heat and light management, demonstrating that, in the case of strong optothermal coupling, the temperature can exceed that of the melting points of both core and shell components. These results demonstrate that the

Received: March 2, 2018
Accepted: March 30, 2018
Published: March 30, 2018

DOI: 10.1021/acs.jpclett.8b00662
J. Phys. Chem. Lett. 2018, 9, 2127−2132

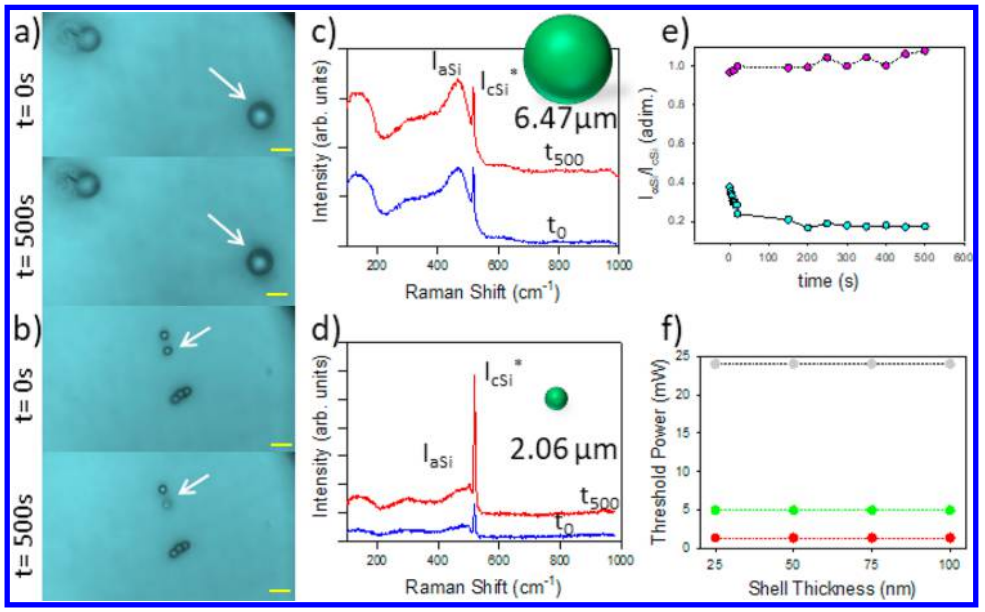

Figure 1. (a,b) Optical images of single SiO_2/Si core/shell beads (Si-rex100) before (upper) and after (lower) irradiation with 633 nm laser beam (laser power: 5 mW; exposure time: 500 s): (a) 6_Si100 and (b) 2_Si100 samples. Scale bars = 5 μm. (c,d) Raman spectra of the samples before (blue) and after (red) 500 s of exposure to the Raman laser beam (laser wavelength: 633 nm, power: 5 mW); (c) 6_Si100 and (d) 2_Si100 samples. (e) Raman intensity ratio (I_{aSi}/I_{cSi}) as a function of time respectively for 6_Si100 (pink) and for 2_Si100 (light blue). (f) Threshold laser power as a function of shell thickness for a single 2_Si100 bead at three different laser wavelength (532 nm (green), 633 nm (red) and 785 nm (gray)).

substitution of plasmonic metals with nonplasmonic enhancers does not ensure thermal stability in SERS analysis. On the other hand, exciting opportunities emerge for heat management at the micro- and nanoscale.

Two different sizes, 2.06 ± 0.05 and 6.47 ± 0.32 μm, of SiO_2 cores and four different values of amorphous silicon (a-Si) shell thickness (25, 50, 75, and 100 nm) were deposited on Si(100) substrates by rf-magnetron sputtering and selected for the study (details in the Supporting Information, SI 1 and SI 2). The laser spot size of the three wavelengths is commensurate with the 2 μm-sized beads, which enables a geometrically efficient light in-coupling. On the other hand, in the case of ~6.5 μm-sized cores, the laser spot size is about 1/3 of that of the whole sphere. Both single beads and three-dimensional (3D) colloidal crystals were analyzed.

Figure 1 compares beads of the two different types of SiO_2 cores coated with a 100 nm-thick shell layer of a-Si (Si-rex100), individually irradiated by a He−Ne laser (λ = 633 nm) with the setup of a typical microRaman experiment (laser power: 5 mW, microscope objective: 100X NA: 0.9, backscattering acquisition).

The optical microscope images show that 6.47 μm-core Si-rex100 beads (from now on: sample 6_Si100) are stable under laser irradiation (Figure 1a), whereas at the same conditions, the 2.06 μm-core Si-rex100 beads (sample 2_Si100) undergo an evident modification of their morphology (Figure 1b), indicating the onset of thermal effects that induce a progressive surface melting until the complete degradation of the bead (see also data reported in SI5 and SI6). This means that the local temperature exceeds the melting threshold of the a-Si (Melting $point_{bulk}$: 1414 °C) and, in the case of prolonged irradiation, even that of SiO_2 (Melting $point_{bulk}$: 1710 °C).[20] This remarkable local heating is similar to that observed for SiO_2/Au beads irradiated with a Raman laser under analogous conditions[21] and demonstrate that, in particular cases, nonplasmonic heating can be as efficient as the plasmonic one. However, we note that, in the case of SiO_2/Au beads, the melting point of gold is lower than that of silicon and becomes further depressed during melting by the formation of core/shell eutectic mixtures, which are not possible in the case of Si-rex samples. The surface melting/reshaping processes were directly monitored by Raman spectroscopy (Figures 1c,d). Figure 1c shows the Raman spectrum of sample 6_Si100 at the beginning of laser irradiation and after 500 s. Both spectra are characterized by the presence of a broad band at around 500 cm^{-1}, which is due to the a-Si shell and a narrow peak at 521 cm^{-1}, representing the contribution of the Si (100) single crystal substrate. No significant differences between the two spectra are observed before and after laser irradiation, which confirms the thermal stability of the beads during the Raman acquisition. On the other hand, the Raman spectra of sample 2_Si100 exhibit a clear evolution as a function of the irradiation time. In particular, the intensity of the Raman mode of the Si substrate (521 cm^{-1}) progressively increases during irradiation, becoming quadrupled after 500 s. In parallel, a-Si becomes partially crystallized, as revealed by the appearance of a small, narrow peak at 501.8 cm^{-1}.[22] This evolution of the Raman spectra agrees with the depletion of the beads observed in optical images, which makes the underlying substrate more accessible to the laser beam. The intensity ratio between the signal of the a-Si shell and that of the crystalline Si substrate is plotted in Figure 1e for both the samples. These data further confirm that the morphology of the 6_Si100 beads remains unchanged and reveal that the evolution of partial surface melting of beads in sample 2_Si100 is stabilized after about 200 s, showing no further progresses for longer irradiation times. Such a different thermal stability strongly suggests a dependence of the opto-thermal effects on the bead size. The optical microscope analysis allows the experimental determination of a laser power threshold, which defines the upper boundary for thermal stability of the beads. Above this threshold, the beads exhibit major morphology modifications. As a result, no reliable

DOI: 10.1021/acs.jpclett.8b00662
J. Phys. Chem. Lett. 2018, 9, 2127−2132

and reproducible Raman analyses can be carried out, yet several possible optothermal applications come into play. Figure 1f plots data of the laser power threshold as a function of different shell thickness for sample 2_Si100 irradiated with the three most common laser sources (532, 633, and 785 nm) for a given time (500 s), reproducing the condition of a generic Raman experiment.

These data reveal that, in the case of 2 μm-sized beads, the differences in shell thickness do not significantly influence the power threshold. However, the pure SiO_2 cores are stable at different wavelengths and even for prolonged irradiation times. This means that the introduction of a thin shell layer of a-Si (e.g., 25 nm) is sufficient to heat up the beads. On the other hand, the comparison with the 6_Si100 sample data reveals that heat propagation is mainly modulated by the size of the beads, which is ultimately determined by the core size. Moreover, the power threshold is strongly dependent on the laser wavelength, reaching a minimum (1.4 mW) at λ = 633 nm. The use of a near-infrared laser source (λ = 785 nm) allows to increase the thermal stability of the beads (power threshold: 24 mW). It is interesting to note that the trend of threshold power cannot be directly predicted from optical simulations of light absorption obtained by considering individual spheres in air (see SI 3). These calculations can only give a qualitative indication of the absorption efficiency at different laser wavelengths. However, from a quantitative viewpoint, the absorption resulted very similar for both 2_Si100 and 6_Si100 systems. This represents a critical issue, suggesting that the computational approaches that are commonly utilized to predict the opto-thermal behavior of these systems on the sole basis of their optical properties might be oversimplified. In particular, they do not take heat propagation into account. On the other hand, the experimental data suggest that the efficient dissipation of heat accumulated upon laser irradiation play a major role on the overall thermal effect. In this regard, it is important to further remark that the size of the beads in sample 2_Si100 is similar to the laser spot size, whereas the 6_Si100 beads are three times larger. This means that, in the latter case, heat generated by laser irradiation can be easily dissipated through lateral propagation and the electromagnetic coupling related to the sphere curvature becomes negligible. Thus, heat accumulated on the 6_Si100 sphere is very low and comparable to that observed for planar thin films. On the contrary, the local fields generated by laser irradiation of sample 2_Si100 are confined within the sphere, and cannot be efficiently dissipated over a larger surface. Moreover, the core/shell geometry does not allow an efficient discharge of the accumulated heat through the underlying substrate. This is not an issue for the 6_Si100 beads, in which the large extension of the area surrounding the laser spot ensures efficient heat dissipation, but becomes critical for sample 2_Si100, which does not have any easily accessible channels for heat dissipation. This situation is further amplified in the case of 3D colloidal crystals.

Figure 2 shows a few examples of the effects of laser irradiation for 3D colloidal crystals made of either 6_Si100 or 2_Si100 beads, respectively. The 6_Si100 3D crystals are thermally stable (Figure 2a), allowing Raman measurements to be carried out without damaging the analytes. For example, Figure 2b shows the spectrum of methylene blue detected from a solution at very low concentration (10^{-9} M). These results are comparable to those obtained with conventional, plasmon-assisted SERS in terms of sensitivity and much better in terms of reproducibility (see SI 4), which corroborates the exciting

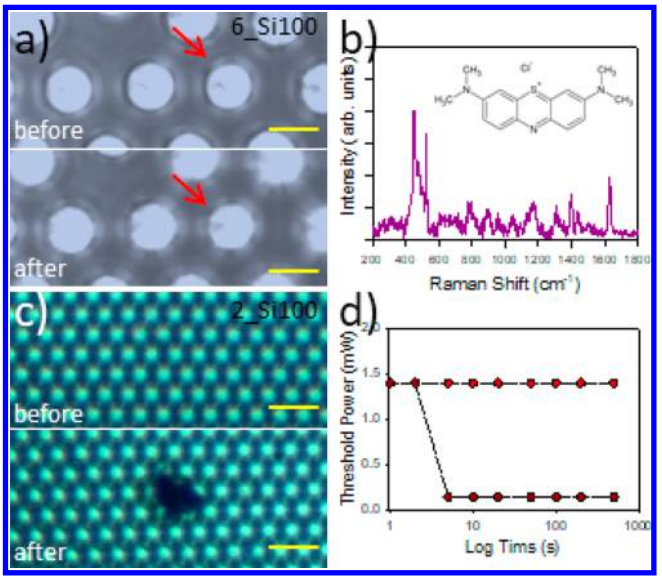

Figure 2. (a) Optical image of a 3D colloidal crystal of 6_Si100 beads before (upper) and after (lower) exposure at λ = 633 nm (laser power: 5 mW, exposure time: 500 s). (b) Example of Raman spectrum of methylene blue 10^{-9} M adsorbed onto the surface of a 6_Si100 3D colloidal crystal. (c) Optical image of a 3D colloidal crystal of 2_Si100 beads before (upper) and after (lower) exposure at λ = 633 nm (laser power: 1.4 mW, exposure time: 500 s). (d) Threshold laser power as a function of time for a single 2_Si100 (red) and a 3D colloidal crystal of 2_Si100 beads (dark red).

scenarios for nonplasmonic SERS that have been envisaged in the introduction.

On the other hand, 2_Si100 samples exhibit clear damages when irradiated for few seconds by a 633 He−Ne laser at low power (1.4 mW) (Figure 2c). We note that the 2_Si100 single sphere samples are stable under the same conditions, which means that the 3D assembly strongly increases the laser-induced heat generation, with consequent lowering of the threshold power by a factor of 10 (from 1.4 to 0.14 mW, Figure 2d and SI5). These data further demonstrate that 2_Si100 samples have a lower thermal stability, which undermines their usefulness for Raman analysis. In this regard, it is important to obtain a more general, synoptic overview of the thermal stability of 3D colloidal crystals made of 2 μm-sized core beads as a function of shell thickness, laser wavelength and irradiation time. Figure 3a shows the threshold power as a function of the Raman laser wavelength (785, 633, and 532 nm) and the a-Si shell thickness at a given irradiation time (500 s). Figure 3b shows the threshold power trend for a given laser wavelength (633 nm) for different a-Si shell layers as a function of the irradiation time (see also SI 6).

These data confirm the existence of a maximum heating generation for the laser irradiation at 633 nm, which results in the lowest laser threshold power. However, unlike the single-sphere counterparts, the 3D colloidal crystals show a stronger dependence of the laser threshold on the shell thickness. In particular, for a-Si shell with a thickness >75 nm, there is a significant decrease of the laser threshold power, even for irradiation at 785 nm, which is the less-heating wavelength. This suggests that the presence of other spheres can further hamper heat dissipation. This is reasonable, as the distance from the heating secondary source (the focal point, located on the top of a sphere, which is in turn placed on the top of the crystal) to the substrate is so large that heat remains trapped

DOI: 10.1021/acs.jpclett.8b00662
J. Phys. Chem. Lett. 2018, 9, 2127−2132

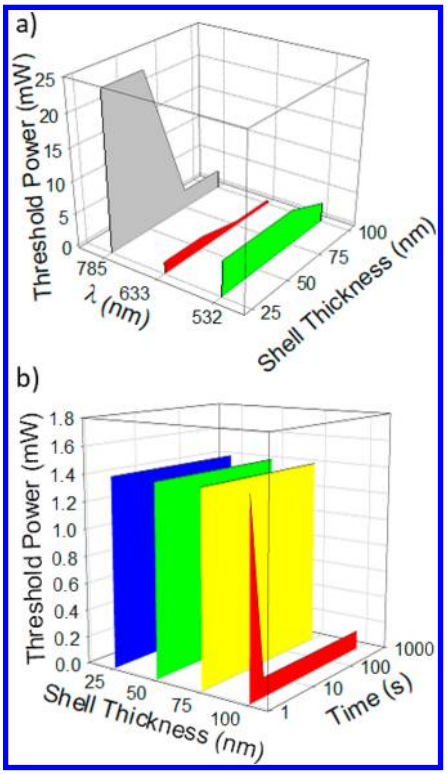

Figure 3. (a) Threshold laser power as a function of shell thickness for a 3D colloidal crystal of 2_Si100 beads irradiated at λ = 532, 633, and 785 nm. (b) Threshold laser power as a function of time for a 3D colloidal crystal of 2_Si beads with different thicknesses (25 nm blue, 50 nm green, 75 nm yellow, 100 nm red) at λ = 633 nm.

within the colloidal crystal. As a result, cumulative heating effects make 2_Si100 3D colloidal crystals very unstable under laser irradiation.

The shell thickness plays a key role also in determining the thermal stability of these 3D systems also as a function of irradiation time. As shown in Figure 3b, the thickest layers (100 nm) do not sustain a 633 nm irradiation at power >0.2 mW for more than 1 s, which makes 2_Si100 beads useless for any practical Raman analysis. On the other hand, this limitation can be turned into an exciting opportunity for applications requiring an efficient light-to-heat conversion at micro- and nanoscale, including laser printing,[23,24] microwelding[25−27] or even photothermal therapy.[28]

Figure 4 shows a couple of examples of laser writing obtained by irradiating 2_Si25 3D colloidal crystals with a 633 nm microRaman laser (laser power: 7 mW, irradiation time: 10 s). It is evident that the good match between the size of the laser beam and that of the beads, together with a judicious control of the laser power and irradiation time enables a precise production of the graphical information that can be printed on the crystals. Analogous results can be obtained using different laser wavelengths (see SI 7).

In conclusion, this experimental study reveals that the size and assembly of SiO_2/a-Si core/shell microbeads are key parameters that can be properly tuned to yield very different opto-thermal properties. Compared to the Si dimer-based antennas recently investigated by Caldarola et al.,[17] which demonstrated excellent thermal stability under laser irradiation, the core/shell SiO_2/Si microbeads exhibit a more complex behavior, requiring a careful design of core size and assembly. However, the usefulness of these results is not restricted to

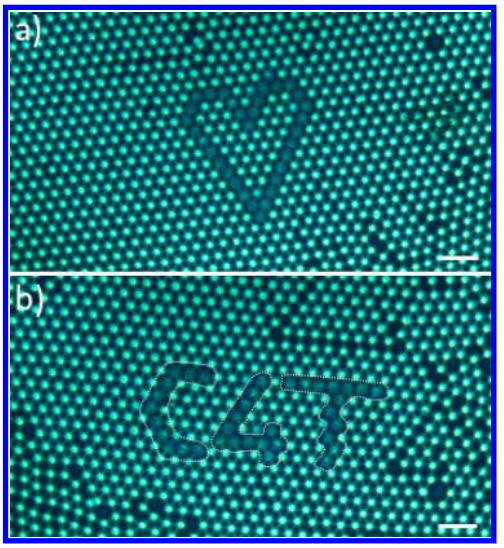

Figure 4. Examples of laser writing obtained by irradiating the 2_Si25 3D colloidal crystals with a He−Ne Raman laser (λ = 633 nm, laser power: 7 mW, exposure time: 10 s per bead). Scale bars: 5 μm. White dots have been added to panel b to define the contour of the written tracks.

core/shell microbeads. Zograf et al. recently demonstrated that in Si nanoparticles the optical field localization at magnetic quadrupolar resonance is able to generate a remarkable optical heating, despite its imaginary part of refractive index is 2 orders of magnitude lower than that of metals.[29] Our study corroborates those observations and provides new insights into opto-thermal management of Si-based systems, demonstrating that the local heating can be increased beyond the melting point of refractory materials. On the other hand, we also demonstrated that thermally robust beads with outstanding nonplasmonic Raman enhancement can be fabricated starting from analogous building blocks with different sizes. These observations open intriguing perspectives in view of producing all-dielectric or hybrid metamaterials with precisely controlled opto-themal activations[30,31] and can stimulate the development of a comprehensive theory of light-to-heat conversion in these systems.[32−36]

■ ASSOCIATED CONTENT

Supporting Information

The Supporting Information is available free of charge on the ACS Publications website at DOI: 10.1021/acs.jpclett.8b00662.

SI 1: Fabrication of SiO_2/Si beads; SI 2: SEM images; SI 3: FDTD simulations of the optical absorption of 2_Si100 and 6_Si100 beads; SI 4: details on SERS experiments; SI 5: light-induced modifications in 3D core/shell Si-rex samples (2_Si series) irradiated at λ = 633 nm: power threshold; SI 6: SEM images of 2_Si samples irradiated at λ = 532 nm (laser power: 50 mW; irradiation time: 1−20 s); SI 7: examples of laser writing by irradiation at λ = 532 nm (PDF)

■ AUTHOR INFORMATION

Corresponding Author

*E-mail:ivano.alessandri@unibs.it.

ORCID

Ivano Alessandri: 0000-0003-0332-0723

DOI: 10.1021/acs.jpclett.8b00662
J. Phys. Chem. Lett. 2018, 9, 2127−2132

Author Contributions

I.A. conceived and supervised the study. N.B. carried out the laser irradiation experiments and analyzed data with the contribution of I.V. P.C. deposited the shell layers. M.F. and M.D. carried out the microstructural characterization. S.D. performed the numerical simulation of the optical properties. All the authors discussed the results and contributed to the final version of the manuscript.

Notes

The authors declare no competing financial interest.

■ ACKNOWLEDGMENTS

We thank Enrico Turrini (University of Brescia) for assistance in data elaboration. This work was carried out in the framework of the project: "Microsfere adattative per il monitoraggio e l'abbattimento di inquinanti persistenti-MI ADATTI E L'ABBATTI" supported by INSTM and Regione Lombardia.

■ ABBREVIATIONS

6_Si100:6.47 μm-core Si-rex100; 2_Si100:Two μm-core Si-rex100

■ REFERENCES

(1) Alessandri, I.; Lombardi, J. R. Enhanced Raman Scattering with Dielectrics. *Chem. Rev.* **2016**, *116*, 14921−14981.
(2) Baffou, G.; Quidant, R. Thermo-Plasmonics: Using Metallic Nanostructures as Nano-Sources of Heat. *Laser Photon. Rev.* **2013**, *7*, 171−187.
(3) Salmistraro, M.; Schwartzberg, A.; Bao, W.; Depero, L. E.; Weber-Bargioni, A.; Cabrini, S.; Alessandri, I. Triggering and Monitoring Plasmon-Enhanced Reactions by Optical Nanoantennas Coupled to Photocatalytic Beads. *Small* **2013**, *9*, 3301−3307.
(4) Zhao, L.-B.; Zhang, M.; Huang, Y.-F.; Williams, C. T.; Wu, D.-Y.; Ren, B.; Tian, Z.-Q. Theoretical Study of Plasmon-Enhanced Surface catalytic Coupling Reactions of Aromatic Amines and Nitro Compounds. *J. Phys. Chem. Lett.* **2014**, *5*, 1259−1266.
(5) Alessandri, I.; Ferroni, M.; Depero, L. E. Plasmon-Assisted, Spatially Resolved Laser Generation of Transition Metal Oxides from Liquid Precursors. *J. Phys. Chem. C* **2011**, *115*, 5174−5180.
(6) Hartman, T.; Wondergem, C. S.; Kumar, N.; van den Berg, A.; Weckhuysen, B. M. Surface- and Tip-Enhanced Raman Spectroscopy in Catalysis. *J. Phys. Chem. Lett.* **2016**, *7*, 1570−1584.
(7) Alessandri, I. Enhancing Raman Scattering Without Plasmons: Unprecedented Sensitivity Achieved By TiO_2 Shell-Based Resonators. *J. Am. Chem. Soc.* **2013**, *135*, 5541−5544.
(8) Bontempi, N.; Carletti, L.; De Angelis, C.; Alessandri, I. Plasmon-Free SERS Detection of Environmental CO_2 on TiO_2 Surfaces. *Nanoscale* **2016**, *8*, 3226−3231.
(9) Bontempi, N.; Vassalini, I.; Alessandri, I. All-dielectric core/shell resonators: From plasmon-free SERS to multimodal analysis. *J. Raman Spectrosc.* **2018**, *49*, 1−11.
(10) Alessandri, I.; Depero, L. E. All-Oxide Raman-Active Traps for Light and Matter: Probing Redox Homeostasis Model Reactions in Aqueous Environment. *Small* **2014**, *10*, 1294−1298.
(11) Alessandri, I.; Biavardi, E.; Gianoncelli, A.; Bergese, P.; Dalcanale, E. Cavitands Endow All-Dielectric Beads With Selectivity for Plasmon-Free Enhanced Raman Detection of Ne-Methylated Lysine. *ACS Appl. Mater. Interfaces* **2016**, *8*, 14944−14951.
(12) Alessandri, I.; Vassalini, I.; Bertuzzi, M.; Bontempi, N.; Memo, M.; Gianoncelli, A. "RaMassays": Synergistic Enhancement of Plasmon-Free Raman Scattering and Mass Spectrometry for Multimodal Analysis of Small Molecules. *Sci. Rep.* **2016**, *6*, 34521.
(13) Ausman, L. K.; Schatz, G. C. Whispering-Gallery Mode Resonators: Surface Enhanced Raman Scattering Without Plasmons. *J. Chem. Phys.* **2008**, *129*, 054704.
(14) Cao, L.; Nabet, B.; Spanier, J. E. Enhanced Raman Scattering from Individual Semiconductor Nanocones and Nanowires. *Phys. Rev. Lett.* **2006**, *96*, 157402.
(15) Bontempi, N.; Salmistraro, M.; Ferroni, M.; Depero, L. E.; Alessandri, I. Probing the Spatial Extension of Light Trapping-Induced Enhanced Raman Scattering in High-Density Si Nanowire Arrays. *Nanotechnology* **2014**, *25*, 465705.
(16) Rodriguez, I.; Shi, L.; Lu, X.; Korgel, B. A.; Alvarez-Puebla, R. A.; Meseguer, F. Silicon Nanoparticles as Raman Scattering Enhancers. *Nanoscale* **2014**, *6*, 5666−5670.
(17) Caldarola, M.; Albella, P.; Cortés, E.; Rahmani, M.; Roschuk, T.; Grinblat, G.; Oulton, R. F.; Bragas, A. V.; Maier, S. A. Non-Plasmonic Nanoantennas for Surface Enhanced Spectroscopies With Ultra-Low Heat Conversion. *Nat. Commun.* **2015**, *6*, 7915−7923.
(18) Albella, P.; Alcaraz de la Osa, R.; Moreno, F.; Maier, S. A. Electric and Magnetic Field Enhancement with Ultralow Heat Radiation Dielectric Nanoantennas: Considerations for Surface-Enhanced Spectroscopies. *ACS Photonics* **2014**, *1*, 524−529.
(19) Dmitriev, P. A.; Baranov, D. G.; Milichko, V. A.; Makarov, S. V.; Mukhin, I. S.; Samusev, A. K.; Krasnok, A. E.; Belov, P. A.; Kivshar, Y. S. Resonant Raman Scattering from Silicon Nanoparticles Enhanced by Magnetic Response. *Nanoscale* **2016**, *8*, 9721−9726.
(20) Donovan, E. P.; Spaepen, F.; Turnbull, D.; Poate, M.; Jacobson, D. C. Heat of crystallization and melting point of amorphous silicon. *Appl. Phys. Lett.* **1983**, *42*, 698.
(21) Alessandri, I.; Ferroni, M.; Depero, L. E. Plasmonic Heating-Assisted Transformation of SiO_2/Au Core/Shell Nanospheres (Au Nanoshells): Caveats and Opportunities for SERS and Direct Laser Writing. *Plasmonics* **2013**, *8*, 129−132.
(22) Aouassa, M.; Mitsai, E.; Syubaev, S.; Pavlov, D.; Zhizhchenko, A.; Jadli, I.; Hassayoun, L.; Zograf, G.; Makarov, S.; Kuchmizhak, A. Temperature-feedback direct laser reshaping of silicon nanostructures. *Appl. Phys. Lett.* **2017**, *111*, 243103.
(23) Zhu, X.; Yan, W.; Levy, U.; Mortensen, N. A.; Kristensen, A. Resonant Laser Printing of Structural Colors on High-Index Dielectric Metasurfaces. *Sci. Adv.* **2017**, *3*, e1602487.
(24) Alessandri, I. Writing, Self-Healing, and Self-Erasing on Conductive Pressure-Sensitive Adhesives. *Small* **2010**, *6*, 1679−1685.
(25) Alessandri, I.; Ferroni, M. Exploiting Optothermal Conversion for Nanofabrication: Site-Selective Generation of Au/TiO_2 Inverse Opals. *J. Mater. Chem.* **2009**, *19*, 7990−7994.
(26) Garnett, E. C.; Cai, W. S.; Cha, J. J.; Mahmood, F.; Connor, S. T.; Christoforo, M. G.; Cui, Y.; McGehee, M. D.; Brongersma, M. L. Self-limited Plasmonic Welding of Silver Nanowire Junction. *Nat. Mater.* **2012**, *11*, 241−249.
(27) King, W. E.; Anderson, A. T.; Ferencz, R. M.; Hodge, N. E.; Kamath, C.; Khairallah, S. A.; Rubenchik, A. M. Laser Powder Bed Fusion Additive Manufacturing of Metals; Physics, Computational and Materials Challenges. *Appl. Phys. Rev.* **2015**, *2*, 041304.
(28) Loo, C.; Lowery, A.; Halas, N.; West, J.; Drezek, R. Immunotargeted Nanoshells for Integrated Cancer Imaging and Therapy. *Nano Lett.* **2005**, *5*, 709−711.
(29) Zograf, P. G.; Petrov, M. I.; Zuev, D. A.; Dmitriev, P. A.; Milichko, V. A.; Makarov, D. V.; Belov, P. A. Resonant Nonplasmonic Nanoparticles for Efficient Temperature-Feedback Optical Heating. *Nano Lett.* **2017**, *17*, 2945−2952.
(30) Rahmani, M.; Xu, L.; Miroshnichenko, A. E.; Komar, A.; Camacho-Morales, R.; Chen, H.; Zarate, Y.; Kruk, S.; Zhang, G.; Neshev, D. N.; Kivshar, Y. S. Reversible Thermal Tuning of All-Dielectric Metasurfaces. *Adv. Funct. Mater.* **2017**, *27*, 1700580.
(31) Chimmalgi, A.; Hwang, D. J.; Grigoropoulos, C. P. Nanoscale Rapid Melting and Crystallization of Semiconductor Thin Films. *Nano Lett.* **2005**, *5*, 1924−1930.
(32) Krasnok, A.; Caldarola, M.; Bonod, N.; Alù, A. Spectroscopy and Biosensing with Optically Resonant Dielectric Nanostructures. *Adv. Opt. Mater.* **2018**, *6*, 1701094.
(33) Yan, J.; Liu, P.; Lin, Z.; Wang, H.; Chen, H.; Wang, C.; Yang, G. Directional Fano Resonance in a Silicon Nanosphere Dimer. *ACS Nano* **2015**, *9*, 2968−2980.

DOI: 10.1021/acs.jpclett.8b00662
J. Phys. Chem. Lett. 2018, 9, 2127−2132

(34) Yan, J.; Liu, P.; Lin, Z.; Yang, G. New Type High-Index Dielectric Nanosensors Based on the Scattering Intensity Shift. *Nanoscale* **2016**, *8*, 5996−6007.
(35) Wu, D.; Yu, H.; Yao, J.; Ma, Q.; Cheng, Y.; Liu, X. Efficient Magnetic Resonance Amplification and Near-Field Enhancement from Gain-Assisted Silicon Nanospheres and Nanoshells. *J. Phys. Chem. C* **2016**, *120*, 13227−13233.
(36) Huang, Z. L.; Wang, J. F.; Liu, Z. H.; Xu, G. Z.; Fan, Y. M.; Zhong, H. J.; Cao, B.; Wang, C. H.; Xu, K. Strong-Field-Enhanced Spectroscopy in Silicon Nanoparticle Electric and Magnetic Dipole Resonance near a Metal Surface. *J. Phys. Chem. C* **2015**, *119*, 28127−28135.

DOI: 10.1021/acs.jpclett.8b00662
J. Phys. Chem. Lett. 2018, 9, 2127−2132